The shadow position sensors (SPS) formation flying metrology subsystem for the ESA PROBA-3 mission: present status and future developments

M. Focardi*[a], V. Noce[a], S. Buckley[b], K. O'Neill[b], A. Bemporad[c], S. Fineschi[c], M. Pancrazzi[a], F. Landini[a], C. Baccani[d], G. Capobianco[c], D. Loreggia[c], M. Casti[e], M. Romoli[d], G. Massone[c], G. Nicolini[c], L. Accatino[f], C.Thizy[g], J. S. Servaye[g], I. Mechmech[g], E. Renotte[g]

[a]INAF - OAA Arcetri Astrophysical Observatory, Largo E. Fermi 5, 50125 Firenze - Italy;
[b]Sensl, 6800 Airport Business Park, Cork - Ireland;
[c]INAF - OATo Turin Astrophysical Observatory, Via Osservatorio 20, 10025 Pino Torinese - Italy;
[d]University of Florence - Dept. of Physics and Astronomy, Largo E. Fermi 2, 50125 Firenze - Italy;
[e]ALTEC - Advanced Logistics Technology Engineering Ctr., C. Marche 79, 10146 Torino - Italy;
[f]AC Consulting, Via Trieste 16/b, 10098 Rivoli, Torino - Italy;
[g]CSL - Centre Spatial de Liège, Liège Science Park, 4031 Angleur, Liège - Belgium.

ABSTRACT

PROBA-3 [1] [2] is a Mission of the European Space Agency (ESA) composed of two formation-flying satellites, planned for their joint launch by the end of 2018. Its main purposes have a dual nature: scientific and technological. In particular, it is designed to observe and study the inner part of the visible solar corona, thanks to a dedicated coronagraph called ASPIICS *(Association of Spacecraft for Polarimetric and Imaging Investigation of the Corona of the Sun)*, and to demonstrate the in-orbit formation flying (FF) and attitude control capability of its two satellites.

The Coronagraph payload on-board PROBA-3 consists of the following parts: the Coronagraph Instrument (CI) with the Shadow Position Sensor (SPS) on the Coronagraph Spacecraft (CSC), the Occulter Position Sensor (OPSE) [3] [4] and the External Occulting (EO) disk on the Occulter Spacecraft (OSC).

The SPS subsystem [5] is one of the main metrological devices of the Mission, adopted to control and to maintain the relative (i.e. between the two satellites) and absolute (i.e. with respect to the Sun) FF attitude. It is composed of eight micro arrays of silicon photomultipliers (SiPMs) [6] that shall be able to measure, with the required sensitivity and dynamic range as asked by ESA, the penumbral light intensity on the Coronagraph entrance pupil.

With the present paper we describe the testing activities on the SPS breadboard (BB) and Development Model (DM) as well as the present status and future developments of this PROBA-3 metrological subsystem.

Keywords: Metrology, Solar Physics, Coronagraph, Formation Flying satellites, SiPM – Silicon Photomultipliers, readout electronics.

*mauro@arcetri.astro.it; phone +39 055 275 5213

Space Telescopes and Instrumentation 2016: Optical, Infrared, and Millimeter Wave, edited by Howard A. MacEwen, Giovanni G. Fazio, Makenzie Lystrup, Proc. of SPIE Vol. 9904, 99044Z · © 2016 SPIE · CCC code: 0277-786X/16/$18 · doi: 10.1117/12.2231699

1. INTRODUCTION

ASPIICS, a classical externally occulted Lyot coronagraph, is the primary payload of the PROBA-3 Mission, studied to provide advanced solar observations in order to achieve two major solar physics objectives: to understand the mechanisms driving the quiescent solar corona behavior and the physical processes leading to coronal mass ejections (CMEs) and to study and predict the so-called "space weather", having a huge impact on several human activities.
PROBA-3 will exploit the formation flying technique applied on the two satellites to form a single giant coronagraph capable of producing a nearly ideal eclipse allowing the observations of the Sun corona closer to the solar limb than ever before.
In nominal formation flying conditions, the two spacecraft Payload reference coordinate frames (OSC-PLF and CSC-PLF), as shown in Figure 1, have the -X axis parallel to the target line (pointing to the Sun), and both spacecraft PLFs are parallel with each other. The distance between the PLFs origins (~144 m) is defined as the nominal Inter-Satellite Distance (ISD). To reach its pre-defined scientific targets ASPIICS shall be operated in nominal FF conditions, where the target direction vector points from the Coronagraph PLF origin to the center of the Sun and both spacecraft PLFs frames are parallel to the -X axis of the Sun Target frame (STF, fixing the roll about the target line).
The CSC satellite will host the coronagraph telescope and the detector to take images of the inner part of the corona in visible polarized light, from 1.08 $R_\odot$ up to about 3 $R_\odot$.
The Coronagraph instrument optical axis will constitute the reference axis for pointing on the CSC, to be aligned along SFT and with the origin of the OSC. To achieve the required opto-mechanical stability, it will be mounted on an optical bench together with metrology instruments and platform attitude star trackers for a first assessment of the spacecraft attitude with respect to the stars.

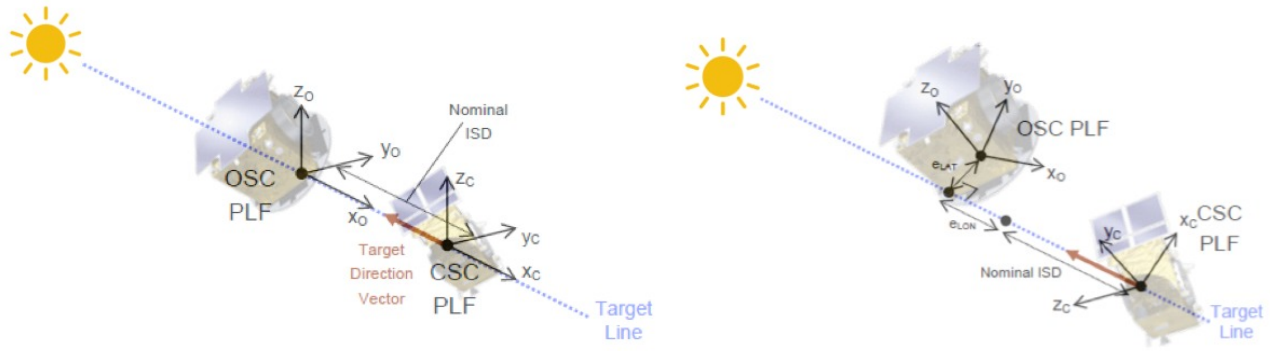

Figure 1: PROBA-3 formation flying satellites with Lateral and Longitudinal position errors shown as defined with respect to the Nominal Formation conditions.

The solar corona will be observed thanks to the presence, on the first satellite facing the Sun, of an external occulter (EO) producing an artificial eclipse of the Sun disk. EO is properly designed [8] to block the light from the solar disk while the coronal light passes through the circular input pupil of the coronagraphic telescope hosted by the Coronagraph Optical Box (COB) and located on the CSC.
The coronagraph aperture center is the origin of the CSC PLF reference coordinate frame, which has a -X axis parallel with the instrument boresight. For the OSC, the PLF reference coordinate frame origin is the center of the occulting disk, and the -X axis of the reference frame is perpendicular to the plane of the disk. The Coronagraph PLF origin is also the center of the formation, and a point on the target direction vector.
The Shadow Position Sensors, composed by 8 SiPM (refer to Figure 2 for their location and orientation), shall measure the absolute position of the EO disk with respect to the entrance pupil of the instrument by verifying the centering of the entrance pupil in the shadow cone of the same EO. To properly perform their function they are accommodated around the coronagraph input pupil plane, limited by a vane of the mechanical flange properly designed to host the SPS readout electronics up to the digitization and communication I/F stages.
The eight silicon photomultipliers are located along a circle having a diameter of 110 mm around the coronagraph entrance aperture. The measurement from each photodiode depends on the position of the photodiode in the umbra/penumbra and is a function of the orientation of the photodiode with respect to the Sun pointing direction. Indeed,

the amount of light reaching the photodiode depends on the effective cross-section of the SPS hole aperture with respect to the Sun direction.

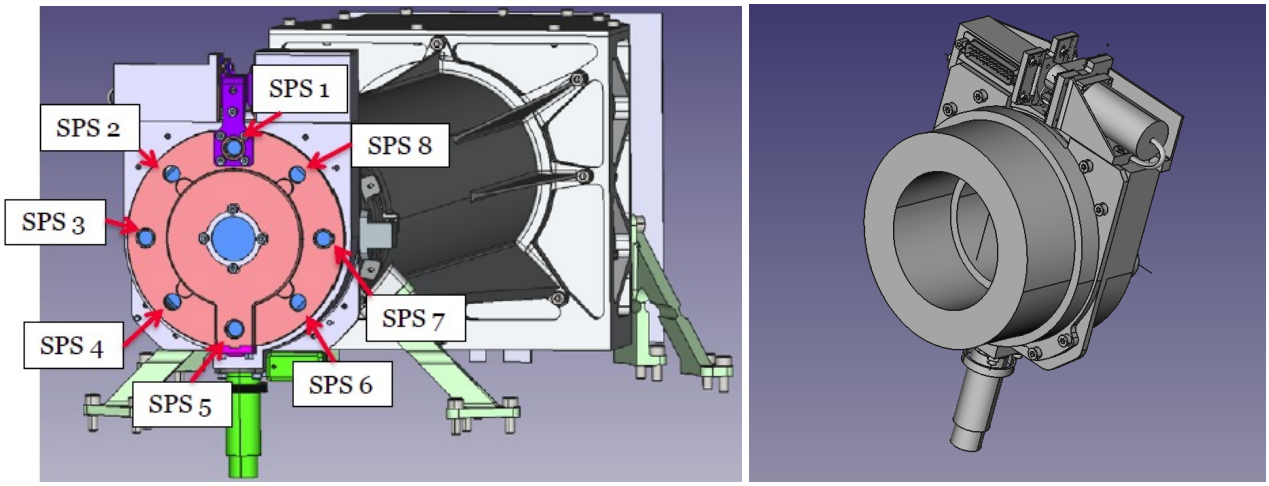

Figure 2: ASPIICS coronagraph and external lid with the holes where are located the SPS sensors (left) and a rear view of the mechanical flange hosting the SPS readout electronics (right) and defining the coronagraph entrance pupil (refer to the internal vane).

2. SPS DESIGN DRIVING REQUIREMENTS

The allowed pointing errors and required accuracies are defined and quantified by means of two main ESA requirements, relevant for the SPS subsystem. In this paragraph we briefly recall these fundamental requirements and summarize the needed sensitivities and dynamic ranges to perform the required measurements, respecting the boundaries indicated by ESA:

A. "SPS performance requirement"

The Shadow Position Sensors (SPS) shall be used to verify that the Coronagraph Instrument's entrance pupil is centered within the umbra cone of the Occulter Disk. At the ISD specified in COR-IIDA-1012[1] and within ±10 mm of the ideal position in lateral and ±100 mm in range, the SPS shall have a lateral measurement accuracy of 50 μm (3σ) in each axis, and a longitudinal measurement accuracy of 1 mm (3σ). These accuracies are with respect to the axis connecting the center of the Occulter with the center of the Sun.

B. "SPS performance goal"

The SPS should be able to return a 3D relative position measurement at reduced performance within a range of ±50 mm in lateral and ±500 mm in longitudinal (i.e. the SPS should always return a 3D measurement within a box of 100 mm in width and height and 1000 mm in depth, centered on the ideal position).

These two fundamental requirements drove Sensl to design the overall SPS readout electronics, defining the required sensitivities and dynamic ranges as well as the so-called *"requirement box"* (20 mm × 20 mm × 200 mm) and *"goal box"* (100 mm × 100 mm × 1000 mm) in which, at the present time, the relevant requirements shall be satisfied.

[1]It is an ESA requirement specified in the Instrument Interface Document (IIDA - Part A) providing the equation to properly compute ISD along the satellites orbit.

Basically, the SPS will provide information on the lateral and longitudinal position of the OSC with different accuracies; for an exhaustive reading on this subject refer to [5].
To determine the SPS required sensitivity and dynamic range we considered the virtual position (i.e. with respect to the umbra center) of the SiPM devices when moving the illumination profile on the SPS plane for the boundaries stated in *A.* in order to determine the minimum required measurable current density variation for the worst case. This happens when the chosen SPS will fall in the nearest location to the umbra. The same considerations are applicable to the determination of the maximum expected value, for the farthest location of a chosen SPS from the umbra limit.
For the identified virtual position, the minimum current density variation is defined as the minimum variation associated to a required displacement of 50 μm transversal or 1 mm longitudinal.
From the penumbra geometrical illumination profile study and the chosen SPS location, we derived the analog required sensitivities (basically current densities variations, being independent from the particular device or from its own area) for the requirement box as reported in the following table:

"SPS performance requirement" (i.e. referred to the requirement box)

Physical quantity	Expected Value	Note
Min current density variation (mA/cm^2)	$2.4\ 10^{-4}$ transversal $2.5\ 10^{-5}$ longitudinal	50 μm transversal 1 mm longitudinal
Min current density (mA/cm^2)	$6.273\ 10^{-3}$	X= +100
Max current density (mA/cm^2)	0.4124	X= -100
Dynamic range (#)	14 bit at least 16245	Nyquist sampling req. 16 bit ADC

Table 1: SPS current densities and dynamic range requirements.

The required dynamic range was found as the current density interval between $6.273\ 10^{-3}$ mA/cm^2 and 0.4124 mA/cm^2. From the same table it can be seen that, at the low end of the range the required sensitivity is 0.025 $\mu A/cm^2$. Therefore, to achieve this sensitivity over the entire dynamic range an ADC with a resolution greater than 14 bits would be needed.

As a design with a 16 bit space qualified ADC have several drawbacks (i.e. they commonly have one only input, a higher cost and are not very common on the market as the commercial, not qualified, equivalent devices), this solution has been discarded in favor of a different design, as provided by Sensl, exploiting a particular SPS readout electronic scheme hosting a 12 bit ADC and a 12 bit DAC as well, as briefly summarized in the following paragraph and fully described in [5].

3. FROM THE EVALUATION BOARD TO THE DEVELOPMENT MODEL

We report in this paragraph the baseline design of the SPS readout electronics as driven by the needed sensitivity and dynamic range indicated in Table 1 that led to the manufacturing of both the SPS Evaluation Board and Development Model.

3.1 SPS baseline design

The design proposed by Sensl is a three-stages amplification chain as shown in Figure 3. The system is based on a double reading of a 12-bit serial ADC that digitizes the voltage of interest and then amplifies its difference with a programmable DC offset that can be set in order to properly cover the needed sensitivities and dynamic ranges as required by both the requirement and goal boxes for the transversal and longitudinal measurements.

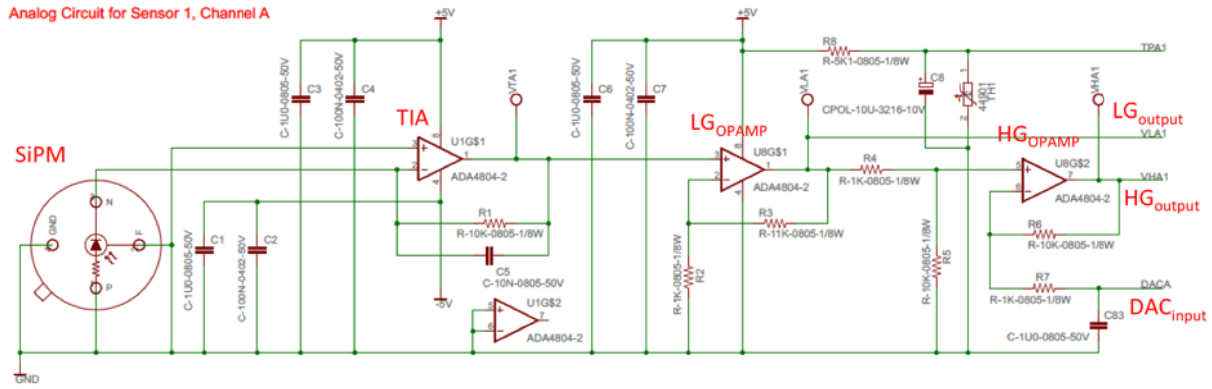

Figure 3: The amplification chain of one SiPM (baseline and DM design).

At the present time the gains in the Development Model (as well as in the Evaluation Board) are selected and distributed among the electronics stages as follows (refer to Figure 3):

1. *Transimpedance amplification (TIA):* A_{TIA}: 10^4 V/A
2. *Low gain amplification (LG):* A_{LG}: 12
3. *High gain amplification (HG):* A_{HG}: 10

A functional scheme showing the conversion between physical quantities and the path followed by their measurements is shown in Figure 4.
The physical quantity that is fed in the SPS algorithms used to control the satellites' relative position is the *irradiance R*, usually measured in W/m^2 or, in our case, mW/cm^2. In the umbra cone (at a distance from the Coronagraph pupil centre less than 38.5 mm) the irradiance is nearly zero (only stray light is present [9]), whereas the sensors will be at full Sun outside the penumbra region. As a reference the solar constant at 1 AU is 137 mW/m^2. At the nominal SPS position (r_{SPS} = 55 mm) the irradiance R is about 1.5 mW/cm^2 including the limb darkening effect that roughly halves the illumination level [7].

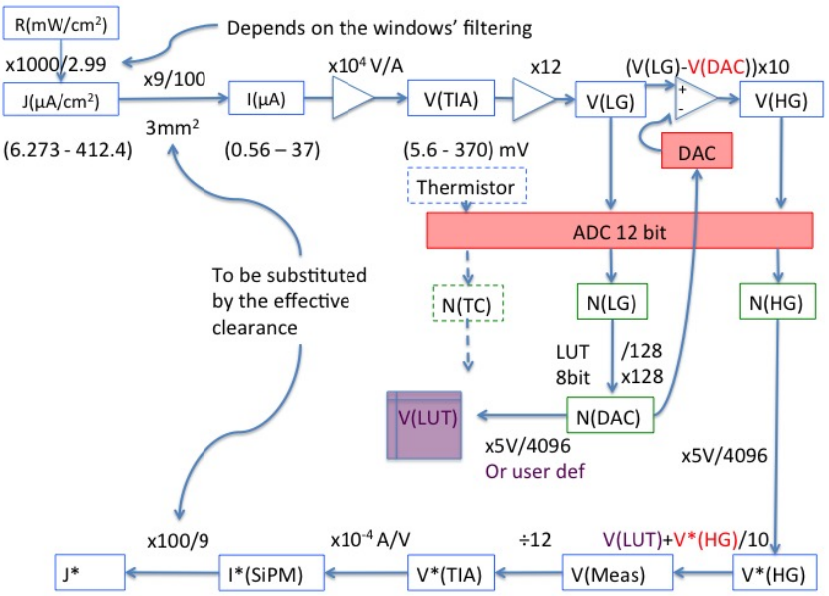

Figure 4: A visual representation of the measurements and signals conversion taking place in the SPS readout electronics. The elements potentially affected by a non-ideal V_A (supply voltage, refer to Par. 5.1) are shown in red and the elements that could benefit from a continuous monitoring of V_A in purple.

These values of irradiance are converted by the SPS system in a current density J measured in μA/cm^2 obtained convoluting the responsivity of the sensor with the spectral solar irradiance. The scale factor that links the irradiance R(mW/cm^2) to the density current J(μA/cm^2) per unit of sensor's surface is, at present, K = 1000/2.99 but it will be reduced by both the filtering effect of the SPS rad-hard windows transmissivity and the coating (that will be presumably applied on the SPS protective window) cutting off the radiation above ~600 nm as the SiPM responsivity varies as a function of the temperature above this particular wavelength.
For what concerns the illuminated area of the sensor we shall also take into account the actual clearance of the SPS pinholes (2.5 mm diameter, as for the flange baseline design).
In the electronic chain the transimpedance amplifier TIA converts the current I in a voltage V_{TIA}, which is amplified by a non-inverting amplifier (gain A_{LG}) in order to generate a signal V_{LG} compatible with the ADC input range 0-5V. For the benefit of this document this shall be known as the LG (Low Gain) amplifier. The output of the LG amplifier is routed to the input of a differential amplifier with gain A_{HG}, and this amplifier will be referred as the HG (High Gain) amplifier.
The voltage V_{LG} is digitized into the 12-bit value N_{LG} that is used to choose the number N_{DAC} with the procedure described in Par. 6.5.
The HG differential amplifier acts on the difference between V_{LG} and the DC offset voltage (V_{DAC}, provided by the DAC) amplifying it by A_{HG} and giving the voltage V_{HG} that is digitized in the 12-bit value N_{HG}.
Each sensor is also monitored by a thermistor with a series resistor across the +5V supply that gives an analog temperature signal also converted to digital by the 12-bit serial ADC and providing so the possibility to perform T calibrations.
A more accurate measurement of the voltage present at the point LG is then calculated as $V_{Meas} = V_{LUT} + V^*_{HG}/A_{HG}$ where V_{LUT} is retrieved from a look-up table. Travelling back, along the SPS electronics chain, we have then: $V^*_{TIA} = V_{Meas}/A_{LG}$

The value written as a result by the application software of the Evaluation Board and of the Development Model in a file .csv (comma separated value) is the current density $J^* = 10/9 \times V_{TIA}$ *(mV)*. This because in both models it is assumed that the illuminated sensor's surface is 9 mm^2 (indeed the SiPM are 3 by 3 mm square devices).
Actually, the algorithms used to reconstruct the position use *irradiances* rather than *current densities*, but the two quantities are linked by a pure scale factor.

The present SPS readout electronics settings are chosen referring to the *requirement box* values only as reported in the Table 1, i.e. in a box ±10 mm lateral and ±100 mm in range, in which the *"SPS Performance Requirement"* (req. A.) asks that a measurement with the needed accuracies shall be performed. As a consequence, the values of the amplification factors chosen to fulfil the requisites inside the so-called requirement box only shall be subjected to a revision, taking also into account the minimum (~0 mA/cm^2, i.e. the stray light level) and maximum (1.77 mA/cm^2) current densities expected inside the *goal box* too.

The first two stages' amplification factors A_{TIA} and A_{LG} were fixed with the aim of exploiting at the best the input range of the last ADC, taking as a reference an uncovered SPS sensors having 3 mm side.
The third (differential) stage amplification factor A_{HG} was chosen instead with the purpose of satisfying the sensitivity (or resolution) requirement: it is such that the minimum longitudinal current variation (25 nA/cm^2 × 9/100 = 2.25 nA) can be resolved by the readout electronics whose ADC LSB analog amplitude is ~1.22 mV (5V/2^{12}).

3.2 Design changes from EB to DM

Some changes have taken place proceeding from the manufacturing of the Evaluation Board to Development Model, as hereunder reported:

- The DM hosts two complete sets of four sensors on a circle of 55 mm radius and is very similar in shape and layout to the final version;
- The OpAmp ADA4804-2, with characteristics very similar to the previous OP484, has been adopted;
- The sensor changed from MICROFB-30035-X05-E26 to MICROFC-30035-X05-E26, same package and comparable performances;
- A separated interface board has been implemented hosting the FPGA implementing the VHDL code.

The reason for changing from a quadruple op-amp to a dual one was to allow the transimpedance amplifier to have the needed dual ±5V supply and, at the same time, to feed the following amplifiers with a single +5V. This, because, if the

differential amplifier has also a -5V supply then when the offset voltage is set greater than the signal, the output tries to drive negative potentially damaging the ADC.
In the interface board a Cyclone III FPGA has been programmed with a first version of the VHDL code.

4. EVALUATION BOARD TESTS

We performed several HW (electrical, functional) and SW tests to take confidence with the experimental setup and the device under test (DUT). The first campaign of measurements regarded:

- Electrical tests (power supply, connections, USB communications, etc.);
- Automatic and manual readout measurements cross-check exploiting the SPS GUI (Graphical User Interface);
- The relative dark level measurements;
- Power supply noise tests with internal and external sources;
- Preliminary tests on the statistical distribution of measurements.

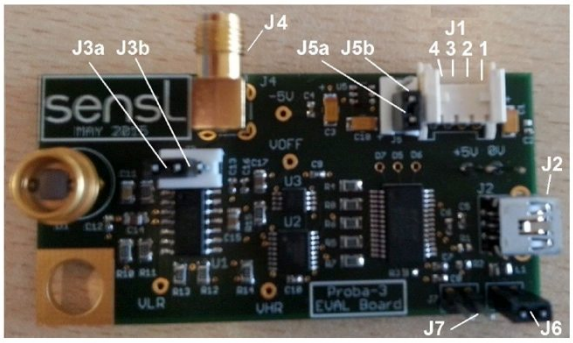

Figure 5: The SPS Evaluation Board.

The experimental setup was firstly arranged placing the Evaluation Board on an optical bench inside a shielded black box for dark level measurements. The other preliminary tests have been performed using a light source, rather constant but not radiometrically calibrated, obtained from a dichroic lamp powered by a bench power supply model DF 1731 SB 3A and a 4-inch integrating sphere. The light from the dichroic lamp was diffused by means of a sheet of Makrolon, 3 mm thick, having a transmission coefficient of about 60%. The light source needs half an hour or more to stabilize its flux when set to a new value.

4.1 Electrical tests

The Evaluation Board is connected to a PC by means of a USB link (J2, refer to Figure 5) that provides also the supply power. There is also the possibility to feed the board with an external +5V through the provided 4-wires connector J1. For this purpose we used a laboratory power supply model IPS-2010.

Without any light, the dark current resulted negligible, in fact the values read by the SW GUI inside the black box gave a result of 0 in every kind of operation: both in manual than in automatic mode.
The total current absorbed resulted about 100 mA including the logic and the USB driver consumption too.

4.2 Functional tests

The main functional test concerned the verification of the consistency of the readings taken in manual or in automatic mode. First of all we checked that the manual readings worked as expected. That is we exposed the sensor to ten different levels of light flux (from zero to saturation) and we took the following set of measures:

1. The LO Res value of the reading;
2. Based on this value we subtracted for the higher values the appropriate pedestal;

3. We checked that the HI Res value was consistent with the LO Res value and presumably a more precise measure of it.

Then we verified that exposing again the sensor to ten levels of light flux from the non-calibrated light source, the automatic readings produced measurements that were proportional to the manual readings with a fixed ratio (5/4096 × 1000/12 × 10/9). With respect to the Development Model in this case it was much easier to perform such a cross-checking because of the presence in the EB GUI of the intermediate value Transimpedance Amplifier Voltage that let us to follow all the measurement steps along the electrical stages.

4.3 EB preliminary statistical tests results

A first estimate of the uncertainties has also been performed. Actually we can report an upper limit only of all the random error contributions because the light source isn't calibrated and its actual stability is unknown.

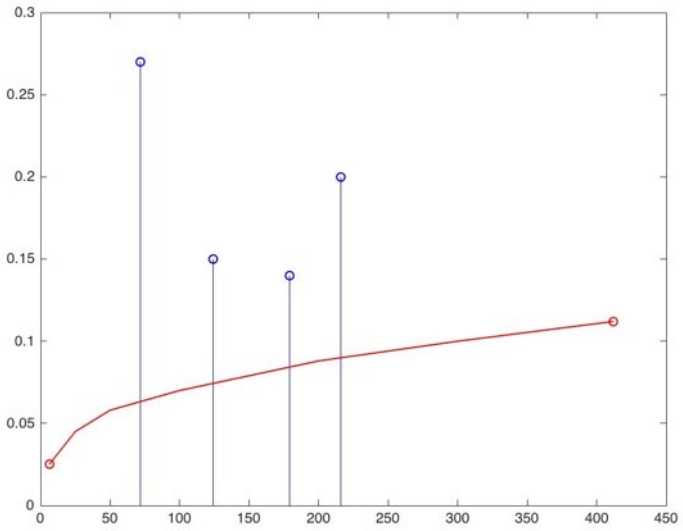

Figure 6: Plot of the standard deviation (1σ) versus the amplitude in μA/cm^2. The red line represents the sensitivities expected in the *requirement box*.

We can observe that the standard deviation of the acquired data is greater than the desired one, also considering that the requirements refer to an uncertainty level of 3σ, so the sensitivity requirement seems not to be accomplished. But these are only preliminary results because they don't take into account the variability in the light flux introduced by the non-calibrated source and they should be better characterized although concerning the not so representative EB.

5. DEVELOPMENT MODEL TESTS

We repeated on the Development Model the same hardware and software tests as for the Evaluation Board and we performed also relative behaviour measurements, placing DM and EB side by side to check their responses.

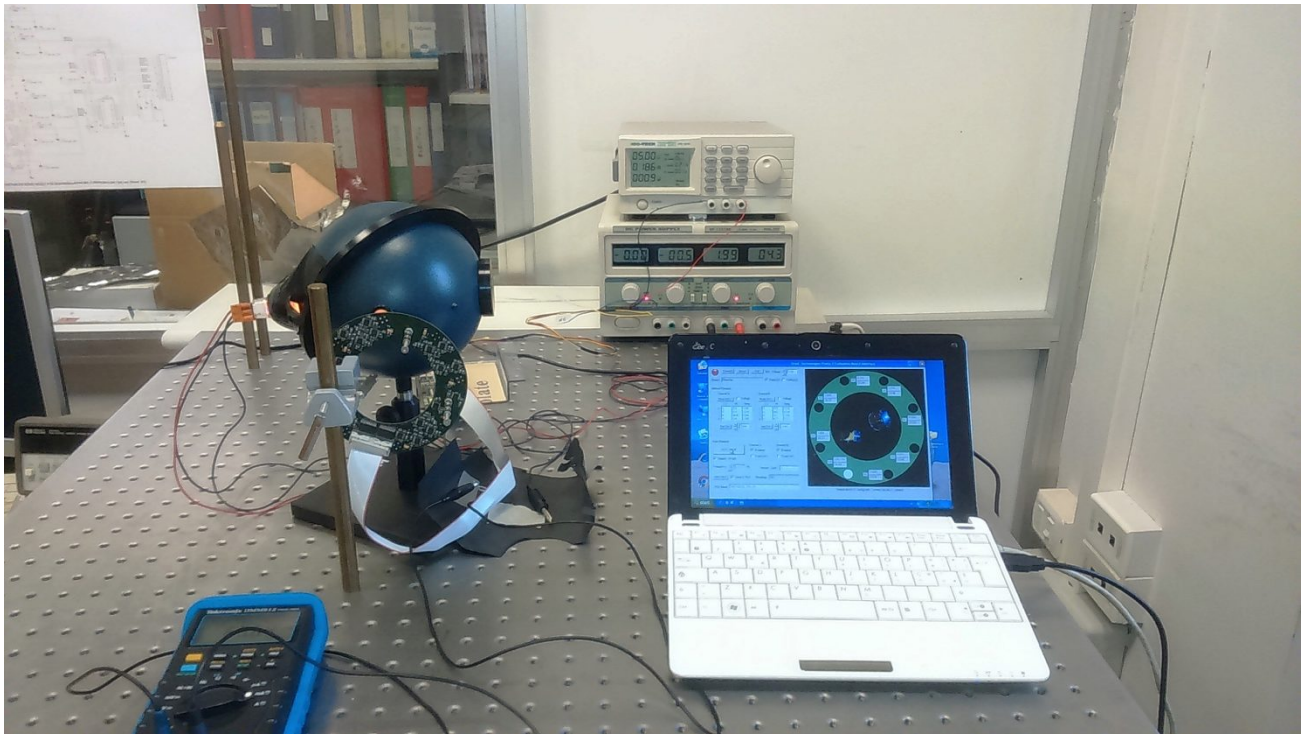

Figure 7: The experimental setup adopted to test the DM (attached, on the left, to the integrating sphere).

5.1 Electrical tests

The dark current resulted negligible, but inside the dark box each sensor gave a different zero level readout: from a minimum of 0.023 μA/cm^2 (equivalent to 2 LSB of the last ADC) to a maximum of 0.226 μA/cm^2 (20 LSB).
The total supply current absorbed by both the DM and the interface board was around 180 mA. The current absorbed by the SPS alone is comprised between 68 and 74 mA for nominal levels of illumination i.e. from darkness to saturation of all the sensors. When the SPS subsystem is exposed to higher light flux such that expected at full sun the absorbed current increments to a maximum of 112 mA.

Voltage supply dependence

The dependence of the readout values from the supplied voltage has been found as purely proportional, as shown in the following Figure 8.
Several measurements campaigns have been taken at different levels of light flux, initially in manual mode, due to a malfunctioning of the automatic readout, then, after SensL fixed this problem, in automatic mode.
The experimental data were taken providing constant light fluxes and consequently fairly constant signals, and varying the supply voltage fed to the DM from a minimum of 4.7 V to a maximum of 5.3 V.
As expected, we have found that the read values depend linearly from the supply voltage, as shown in Figure 8. This behaviour observed in the experimental measurements is described by the equation:

$$V(meas) \cong V(LG) \cdot \left(1 \mp \frac{\Delta V_A}{V_A}\right) \quad (1)$$

This result is of paramount importance in the considerations we will make in the following chapters about the SPS readout electronics dependence from the supplied voltage.

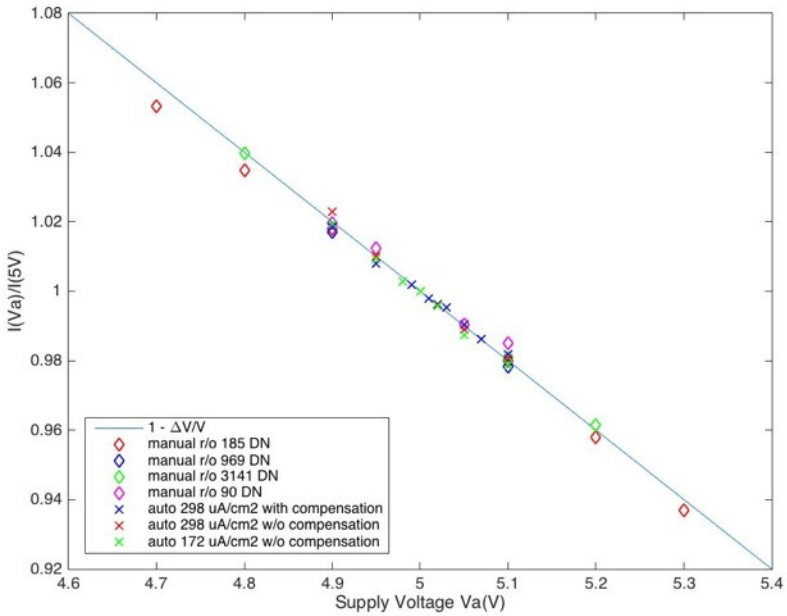

Figure 8: Experimental data showing that any variation of the supplied voltage produces an equivalent variation of the response. The various colours represent different levels of light flux.

5.2 Functional tests

We performed the same functional tests as for the Evaluation Board during which we identified some minor problems, mainly due to the ASW. In particular, the compensation implemented in the DM's GUI by means of the field Ref. Voltage**,** didn't work properly as can be deduced from Figure 9. This defect will be further investigated, but it doesn't affect the other tests results. In fact it is a feature of the DM interface only that won't be implemented in the flight version of the VHDL code.

A more serious anomaly was found consisting in a departure from the ideal behavior when the SPS DM is operated in *automatic mode*. The nature of the problem and its solution are described in detail in the next chapter. At the beginning, the use of the automated readout was precluded because of this malfunction, so the first campaigns of measurement have been done taking bunches of 50 samples in *manual mode* and reporting the results as $N_{DAC} + N_{HG}/10$.

5.3 DM preliminary tests results

We have performed an estimate of the uncertainties similar to what we did for the Evaluation Board case. In Figure 9 are reported the values of the standard deviation versus the amplitude in $\mu A/cm^2$.

Waiting for the tests that will be done in Turin (ALTEC/OATo OPSys facility, [10]) using a calibrated source, we can only report an upper limit of all the random contributions of error, not knowing how relevant the contribution of the variability of our light source is.

In this case we obtained better results with respect to the ones coming from the Evaluation Board. As usual 1σ values of standard deviations are indicated instead of 3σ. The requirement on the sensitivity is obviously better accomplished for the higher values, suggesting that the greatest attention should be placed on the low-end values. For the lower values, up to the minimal intensity of the flux of interest, the sensitivity shall be accurately investigated.

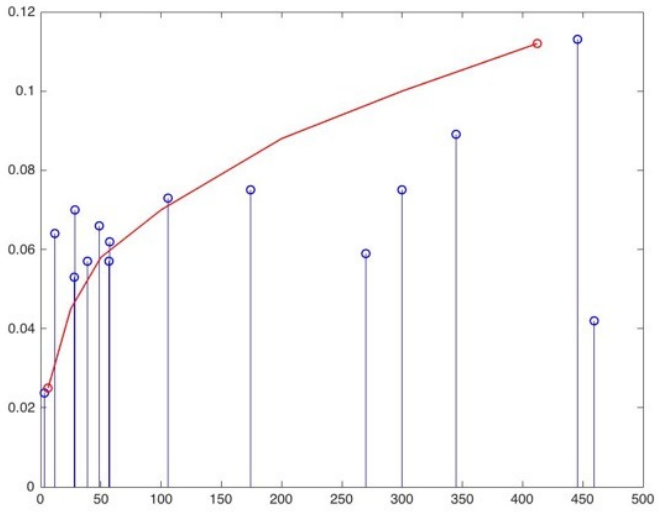

Figure 9: Plot of the standard deviation (1σ) versus the amplitude in μA/cm^2. The red line represents the sensitivities expected in the *requirement box*.

6. LESSONS LEARNED AND DESIGN IMPROVEMENTS/UPGRADES

6.1 The automatic reading anomaly

Just at the beginning of the first tests we noticed an anomalous behaviour when the Development Model was operated in *automatic mode*. The values reported by the GUI, from about 80 μA/cm^2 up to the saturation (which occurs at about 496 μA/cm^2 with the current settings) didn't vary in a uniform way but rather assumed discreet values spaced by about 14 μA/cm^2. Summarising, apart for some details in the low end, the entire system behaved as a 5-bit ADC.
This effect was present on all the sensors with the same values and spacing, hinting that the problem was in the software and not in the electronic chain. The *manual* readings instead didn't suffer of this discretization and their values varied in a continuous mode provided the luminosity grew by little quantities.
To make a comparison, the Evaluation Breadboard was simultaneously illuminated and behaved as expected.

The anomalous behavior solution

SensL was immediately warned of this anomaly and they worked on a new version of the DM application software and of the FPGA VHDL code to solve the problem.
The procedure for the solution of this abnormal behaviour consisted in:

- Removing eight capacitors: to cope with the timing issues;
- Replacing the application SW with a new version (currently 1.02);
- Updating the *Cyclone® III* FPGA by means of the USB-blaster™ and of the Quartus® environment from Altera®.

6.2 The power supply dependence

Another major issue identified during the tests concerns the SPS susceptibility to the supplied voltage mean level and to its variations (noise, ripples, different time-scale variations).
The SPS output values depend from the quality of the supplied voltage and its non-ideality because, in the current design, the voltage reference is tied to the supply voltage V_A for both the DAC and the ADCs.
The influence of an exact knowledge of the supply voltage V_A is twofold:

1. If V_A changes, the DAC voltage subtracted before the last amplification stage changes proportionally;
2. The values read from the ADC are inversely proportional to the V_A level.

All the digital readings from the ADCs depend on V_A so, if we need a calibrated measure of the light (as required by the algorithms), we cannot avoid knowing the actual value of the supply voltage with the needed accuracy in order to correct the value at software level. But, anyway, all the noise contributions on the supply line and its deviations from a stable value will reflect proportionally on the SPS measurements/readouts.

Possible solutions to the power supply dependence issue

The formula (1) of Paragraph 5.1 implies that every uncertainty on the +5V supply voltage line (due to the lack of knowledge of its mean value, to the ripples etc. and to the noise too) reflects entirely on the readout values. This problem can be addressed following one (or more) of the present itemized ways:

1. Specifying stringent requirements on the power supply voltage;
2. By means of a software correction based on the knowledge of the actual value of the supply voltage;
3. Introducing a voltage reference in the design.

The first solution should be compared with the accuracy of the power supplied by the PCU (the PROBA-3 Power Conditioning Unit, in charge of CBK – Centrum Badań Kosmicznych, Space Research Centre of the Polish Academy of Sciences): the provided maximum voltage uncertainty of ±50 mV is not compliant with the SPS needs and should be improved. Moreover, great care should be taken routing a so accurate voltage supply from the origin in the PCU to the final destination in the SPS (cables with a length of ~1.5 m are foreseen).

We can comfortably state that a high frequency noise content, provided the mean level doesn't change, could be filtered by taking multiple measurements or introducing a low pass filter (the RC feedback network of the transimpedance amplifier already acts as a Low Pass Filter – LPF); also the mean value could be corrected, if an adequately precise measurement of it would be possible. But the intermediate frequency content, i.e. expected as slow temporal variations, cannot be corrected after the data has been collected.

Regarding a possible software correction, we note that it should be based on the exact knowledge of the supply voltage in real-time (or quasi real-time) raising a lot of doubts regarding the timeliness of the measurements. More, this will represent an additional load on the computational resources, but, also providing the SPS SW/FW with the present secondary measurements accuracies and resolutions, these would not suffice. In this case the voltage measurements accuracy on board the PCU should be improved too.

Documentation relative to the adopted ADC (ADC128S102QML) and DAC (DAC121S101QML), recommend the usage of the voltage reference component LM4050. This device, as well as other similar space-qualified components, is characterized by a rather bulky package (10-Lead Ceramic CLGA package for the LM4050, TO-5 and TO-46 for others) and this will represent a challenge for a future review of the SPS PCB design. Another difficulty is represented by the need of a further voltage > 5V (+12V - TBD) to be supplied beside the ±5V, or by the introduction of an LDO (Low dropout regulator) on the SPS PCB so to generate the +5V on-board from the +12V. The first solution would imply an additional wire in the harness connecting the PCU to the SPS and the second additional components with extra power consumption.

In order to obtain a proper estimate of the expected effects we performed a numerical simulation, whose result is shown in Figure 10, comparing:

1. A system, as the present one, in which the reference voltages of both ADC and DAC are tied to a supply voltage having the characteristics foreseen for the PCU;
2. A separated V_{REF} supplied from a voltage reference with 0.1% accuracy and a 100μV rms noise (LM4050, worst case);
3. An ideal 5V reference.

From this simulation it is evident that the intrinsic noise introduced by a voltage reference component would have a minimal impact on the overall noise compared with that deriving from a remote supply voltage. On the other side, also increasing by five times the power supply stability, down to +5V ±10 mV (but it seems that this is not feasible – CBK – to SensL private communication), we wouldn't get the voltage reference performances.

For all these reasons, we consider as mandatory the adoption of a voltage reference stabilizing the power supply coming from the PCU to be integrated in the SPS design and feeding the ADCs and DAC V_{ref}.

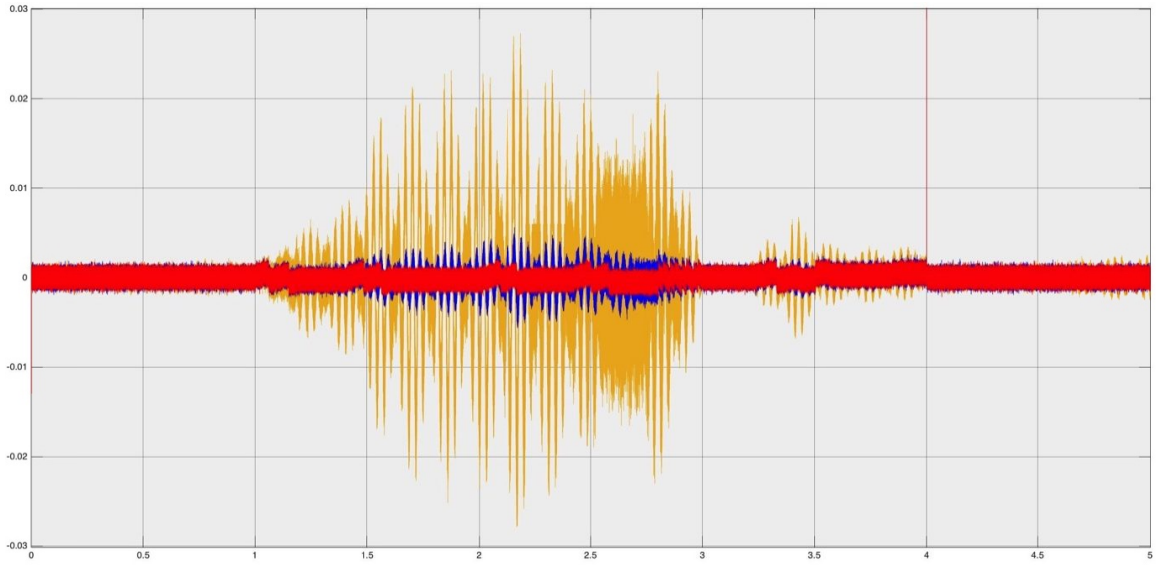

Figure 10: Comparison between the residuals in V in function of the time, obtained in three cases: $V_{REF} = V_A$ as in the current design (yellow plot), with a V_{REF} tied to a Voltage Reference (blue plot) and an ideal 5V reference (red plot). The values at both ends refer to situations where no subtraction from DAC occurs. Between 1.5 and 3 seconds are present higher values for which a pedestal set by DAC is subtracted.

6.3 Dynamic range

We have seen how the dynamic range can be established by setting appropriately the amplification factors A_{TIA} and A_{LG} in the two first stages of the SPS readout electronics. The present amplification factors on the SPS DM readout electronics ($A_{TIA} = 10^4$ V/A and $A_{LG} = 12$) are chosen in function of the needed dynamic range for the so-called *requirement box* only, presuming that all the radiation flux hits the entire 3x3 mm^2 surface of the sensor. The density current values presently expected are the ones reported in Figure 10, top. In this situation the DM is able to satisfy the *"SPS Performance Requirement" (A.)* alone, with a 12% margin.

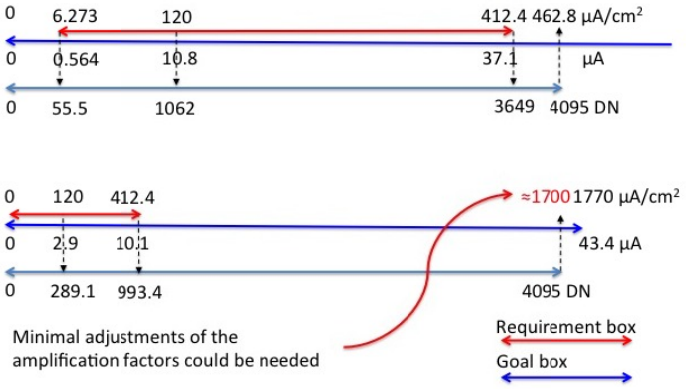

Figure 11: The two pictures show: how the present density current levels calculated in the *requirement box* fit in the dynamic range (top), and how the reduced density current levels (filter cutting 50% of the flux and pinhole diameter of 2.5 mm) calculated for both *requirement box and goal box* almost fit in the dynamic range (bottom), with the current electronics settings.

In the flight version of the SPS subsystem, an important constraint concerning the dynamic range will be the *"SPS Goal Requirement (B.),* establishing the condition of "non-saturation" for the measurements performed inside the so-called *goal box*, so in the next models the gains shall be tuned accordingly to this additional constraint. In this case we must also consider the likely presence of a coating on the SiPM rad-hard windows filtering the red part of the solar spectrum

(λ < 650 nm, TBC), whose transmissivity is TBD and the actual throughput of the SPS pinholes located on the mechanical flange, as already anticipated.

For a given irradiance calculated at a given position, if the electronics should not change, the decreasing of the current generated by the SiPM, caused by a reduced efficiency and/or a reduced illuminated area, goes in the direction of expanding the dynamic range. From the other side, if the minimum current signal to be detected reduces there is a detrimental effect on the fulfilment of the sensitivity requirement. Supposing a 73% drop in the illumination (due to the low-pass filter and to a very likely SPS effective pinhole diameter of 2.5 mm), it is shown in

Figure 11 that, in case we leave the same amplification factors as in the DM (eventually needing only little adjustments), the *"goal"* requirement can be satisfied too.

6.4 Improving the sensitivity

The programmable offset design allows us to obtain an effective resolution far beyond 1 LSB. In fact the number of quantization levels attainable by the system, after the last stage ADC, is equal to: $2^{12} \times A_{HG}$. In the present configuration (with A_{HG} = 10) the minimum output that can be represented is $1/10^{th}$ of LSB = 5V/(4096×10) = 0.122 mV that corresponds to an input current of 1.017 nA. This means that the minimum signal expected to be detected in the previous configuration: 2.25 nA (25 nA/cm^2 × 9 mm^2) was equivalent to about 2.2 quantization levels.

But the minimum level of the signal to be detected will realistically reduce, because of the anticipated reduction of the light flux; so it will be necessary to increase the number of quantization levels. This can be done, apart from all the considerations about the noise, leaving untouched the first two amplification factors and increasing only the value of the last amplification stage A_{HG}.

There is a theoretical limit for A_{HG} given by the number of pedestals that can be subtracted: in fact the present algorithm segments the 5V range in 32 (# TBC) intervals with an amplitude of 5V/32 = 156.25 mV so, the input of the differential stage, will be limited between 0 and 156.25 mV. If we don't want to saturate the ADC we must keep $A_{HG} \leq 32$. However, increasing the number of pedestals from 32 to 64 or more, the value of A_{HG} can be raised too. The only inconvenience is having a longer look-up table (that shall be properly on-ground calibrated).

The main benefit that will be obtained with all these modifications will be an overall resolution for the entire system that changes from $1/10^{th}$ of LSB to a lesser fraction and this will be useful to counteract the effect of the expansion of the dynamic range.

6.5 A smarter algorithm

The number N_{DAC} used to set the DAC originates from the voltage V_{LG} that is digitized in the 12-bit value N_{LG}. The simple method currently adopted to select one the present 32 offset values N_{DAC} is to take the multiple of 128 immediately lesser than N_{LG} thus giving the values from 0 to 31×128. In the Development Model application software, the analog voltages V_{LUT}, corresponding to the 32 discrete values N_{DAC} are automatically generated when the program that manages the DM is installed ($V_{LUT} = N_{DAC} \times 5/4096$ rounded to three decimal places) and written in a text file that can be modified by the user to set the values derived from a calibration procedure. The VHDL code utilizes then this file to translate one of the 32 discrete values N_{DAC}, coded as an 8-bit value, into the corresponding V_{LUT} voltage used to reconstruct $V_{Meas} = V_{LUT} + V^*_{HG}/A_{HG}$ with $V^*_{HG} = N_{HG} \times 5/4096$. The asterisk marks the measured voltages.

Concerning the current choice algorithm we can itemize some important points:

- There is the risk of having a negative value at the input of the last ADC because N_{DAC} is chosen based on a value N_{LG} that comes from a previous reading with respect to N_{HG}. In case of a little initial difference between N_{LG} and N_{DAC} and of a decreasing signal, the value N_{HG} could be read as 0 regardless of the true value of N_{LG};
- Only the part between 0 and 1270 of the entire ADC dynamic range is exploited for representing N_{HG};
- Only values multiple of 128 are written on the DAC as N_{DAC}, unless we had previously calibrated 32 different values on V_{LUT}.

We already pointed out that to get a better resolution (enhancing the sensitivity of the measurements) we can increase the amplification factor of the last (differential) stage from A_{HG} = 10 to 20 or more.

If we want to solve the first issue we can keep the output opportunely centred taking N_{DAC} = 0 for the first interval and subtracting an opportune offset for a non-zero pedestal. This would lead to substitute the current algorithm for the pedestal choice with one slightly more complicated and also the procedure to reconstruct V_{Meas} will become more demanding.

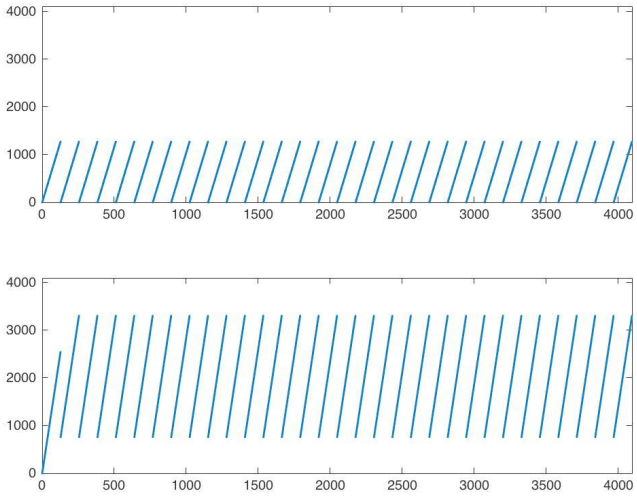

Figure 12: *N(HG)* versus *N(LG)* spanned with the current algorithm (top) and in the suggested configuration with a differential amplification factor of 20 (bottom).

7. SIMULINK MODEL AND PERFORMED SIMULATIONS

Various simulations have been implemented using the Matlab®/Simulink® software package. We started replicating a single sensor and its amplification chain to study separately the contributions from the sensor current noise and from the electronics noise (OpAmp and resistors).
Then we performed a comparison between the current design and an enhanced version for what concerns the immunity to supply voltage variations.
In the next future we will replicate all the system's steps bringing from the illumination levels produced by an arbitrary SPS displacement to the reconstructed position.

7.1 Sensor and amplification chain

Indeed the complete model could not be used to build also moderately complex systems because the simulation time grew too much. So preliminarily it has been performed a comparison between the complete model and a simplified one constituted simply adding a band limited white noise source to the input signal. For all the subsequent simulations concerning the comparison between different reference voltages, the simplified model was used.

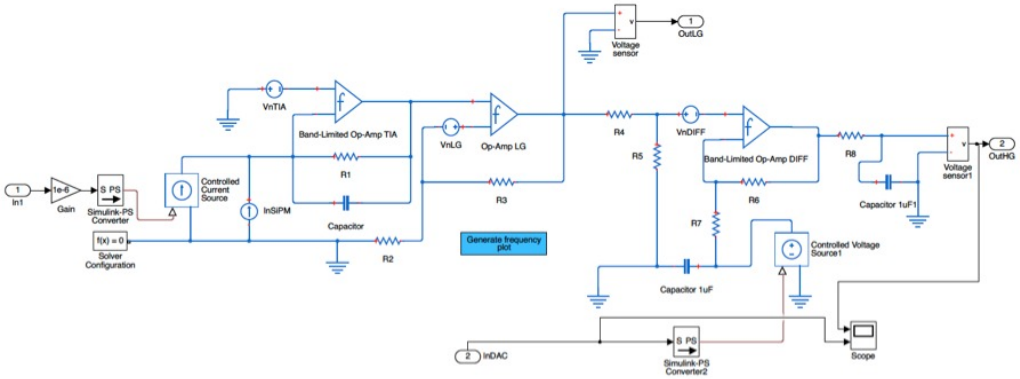

Figure 13: The Simscape/Simulink model of a complete amplification chain used to evaluate the noise produced by a SPS sensor and by its electronics.

7.2 Comparison between different Voltage Reference options

The model has been used to discriminate between two different scenarios: relying on the current design or asking for the introduction of a voltage reference. For this purpose we compared these two alternatives to the ideal case in which only the noise contributions from the sensor and the electronic chain are present. The three configurations are the following:

1. VREF = VA with VA obtained modulating the +5V supply with frequencies of 200, 20 and 2 rad/s (imitating medium time-scale variations) and adding white noise up to obtaining a signal whose value Vpp is comprised between 5V ± 50 mV;
2. VREF coming from a voltage reference with 100 μVrms (10Hz – 10kHz) noise and a 0.1% uncertainty (refer to the LM4050 datasheet, worst case);
3. An ideal 5V reference.

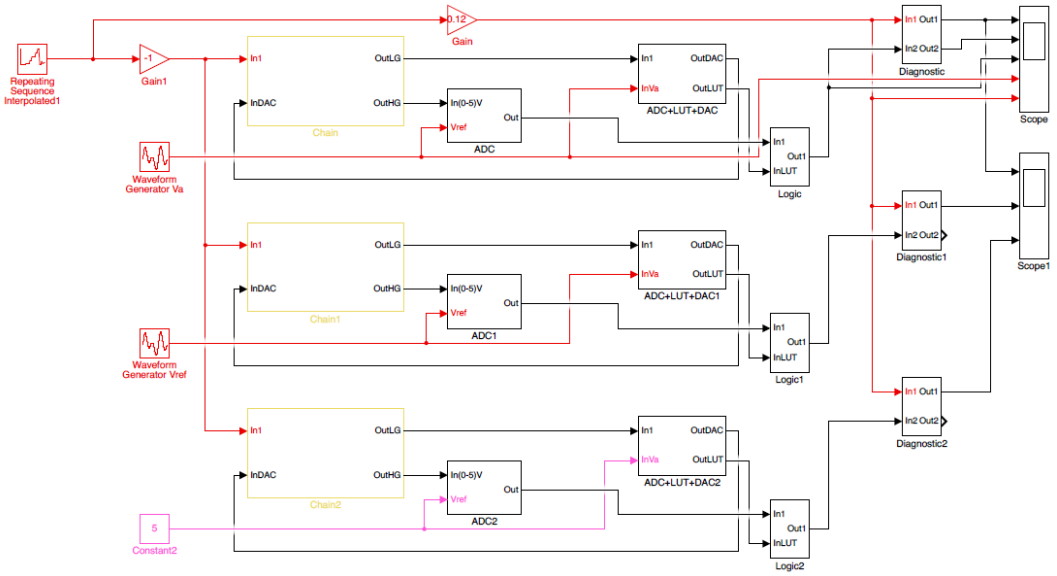

Figure 14: The Simulink model used to analyse the influence of the voltage supply uncertainties on the amplification chain of one SPS sensor.

The residuals originating from the three designs are reported in Figure 10.

7.3 Modeling the light profile

The next step will be to simulate the changes in the illumination profile produced by a generic movement of the SPS with respect to the nominal position. The signals originated by these displacements will be fed to the electronic chains and the calculated irradiances will be used to validate the algorithms used to reconstruct the SPS position.

8. CONCLUSIONS

In this paper we have illustrated the tests performed on the EB and DM readout electronics of the SPS subsystem on board the PROBA-3 Mission. The preliminary results have been put in relation with the SPS relevant requirements, permitting us to make some considerations that could potentially lead to future changes and improvements in the electronics and software design. In particular we described the amplification factors choice criteria w.r.t. the required sensitivity and dynamic range as well as the dependence of this fundamental metrological subsystem from the supplied voltage stability.

9. ACKNOWLEDGMENT

A special thank to the European Space Agency (ESA) for the support provided by the PROBA-3 Management and Technical Staff and for the financial support concerning the contract with CSL and subcontractors, subscribed for the Payload Instrument design and development (B2/C Phases).

REFERENCES

[1] Renotte E. et al., "ASPIICS: an externally occulted coronagraph for PROBA-3. Design evolution", Proc. of SPIE Vol. 9143, 91432M, (2014).
[2] Renotte E. et al., "Design status of ASPIICS, an externally occulted coronagraph for PROBA3", Proc. of SPIE Vol. 9604, 96040A, (2015).
[3] Loreggia D. et al., "OPSE metrology system on board of the PROBA3 mission of ESA", Proc. of SPIE, Vol. 9604 96040F-1, (2015).
[4] Loreggia D. et al., "Characterization of the ASPIICS/OPSE metrology sub-system and PSF centroiding procedure", Proc. of SPIE AT+I, (2016).
[5] M. Focardi et al., "Formation Flying Metrology for the ESA-PROBA3 Mission: The Shadow Position Sensors (SPS) silicon photomultipliers (SiPMs) readout electronics", Proc. of SPIE, Vol. 9604 96040D-1, (2015).
[6] Jackson C., O'Neill K., Wall L., Mc Garvey B., "High-volume silicon photomultiplier production, performance, and reliability", SPIE Optical Engineering 53(8), 081909, (2014).
[7] Bemporad A., Focardi M., Capobianco G. et al., "The Shadow Positioning Sensors (SPS) for Formation Flying Metrology on-board the ESA-PROBA3 Mission", Proc. of SPIE, Vol. 9604 96040C-1, (2015).
[8] Landini F., Bemporad A., Focardi M. et al., "Significance of the occulter diffraction for the PROBA3/ASPIICS formation flight metrology", Proc. of SPIE, Vol. 9604, 96040E, (2015).
[9] C. Baccani et al., "Preliminary evaluation of the diffraction behind the PROBA-3/ASPIICS optimized occulter", Proc. of SPIE AT+I, (2016).
[10] G. Capobianco et al., "The satellite formation flying in lab: PROBA-3/ASPIICS metrology subsystems test-bed", Proc. of SPIE AT+I, (2016).